Research Article

Effective removal of Sb(V) from aqueous solutions by micro-electrolysis with composite scrap iron-manganese as filler

Shangkun DING[1], Saihua HUANG[2], Yiping ZHANG[1], Yongchao ZHOU[1✉]

[1]*Institute of Municipal Engineering, Zhejiang University, Hangzhou 310058, China*
[2]*Zhejiang University of Water Resources and Electric Power, Hangzhou 310018, China*

Abstract: Micro-electrolysis (ME) technology is investigated for improving the efficiency of removal of pentavalent antimony (Sb(V)) from the environment,. In this study, an ME system composed of scrap iron filings, waste manganese fillings, and activated carbon (Fe-Mn-C ME) was used to efficiently remove Sb(V). The results proved that, compared with conventional iron-carbon micro-electrolysis (Fe-C ME), Fe-Mn-C ME significantly enhances the removal rate of Sb(V) when the hydraulic retention time is 10-24h. The Fe-Mn flocs produced by this system were analyzed using XRD, EDS, XPS, and BET surface area analysis, which revealed that the flocs were mostly Mn-substituted FeOOH and had a relatively larger specific surface area, providing better adsorption performance. Furthermore, it was found that the removal rate of Sb(V) decreased as the iron-to-carbon mass ratio increased, while it first increased and then decreased as the manganese content increased. The reduction of Fe(Ⅲ) was accelerated with an increase in the addition of manganese, leading to an increase in the concentration of Fe(Ⅱ). The electron transfer and the formation of Fe(Ⅱ) were facilitated by the potential difference between manganese and carbon, as well as by the formation of microcells between iron and manganese, which improved the reduction ability of Sb(V). From our thorough investigation and research, this is the first report that has proposed Fe-Mn-C ME for removing antimony. It provides a novel approach and technological support for removing Sb(V) efficiently.

Key words: Antimony; Iron; Manganese; Micro-electrolysis; Electrochemistry; Mechanism

1 Introduction

In recent years, the increasing use of antimony (Sb) and its compounds in the textile and dyeing industry has heightened societal concerns regarding antimony pollution (Fei et al., 2017). Antimony and its compounds exhibit toxic and carcinogenic properties towards living organisms. As a result, the United States Environmental Protection Agency (USEPA) and the European Union (EU) have classified antimony as a priority pollutant for regulation (Ungureanu et al., 2015). Despite these measures, antimony pollution remains a critical issue.

✉ Yongchao ZHOU, zhoutang@zju.edu.cn

Under oxidizing conditions, antimony primarily exists in the form of Sb(V) (Mitsunobu et al., 2010), which is more soluble than Sb(III) (Ozdemir et al., 2004). This high solubility makes it difficult to achieve the desired removal rates using conventional water treatment processes (Kang et al., 2003; Guo et al., 2009; Zhou et al., 2022). Consequently, the need for a cost-effective method to remove Sb(V) is urgent.

Sb(V) removal from aqueous solutions has been studied using various methods, including adsorption (Hasan et al., 2021), coagulation-precipitation (Gannon and Wilson, 1986), ion exchange (Riveros et al., 2008; Hasan et al., 2021), membrane separation (Saito et al., 2004; Li et al., 2018), and electro-flocculation (Zhu et al., 2011; Song et al., 2015). Among these, adsorption and coagulation-precipitation are the two most widely used techniques. Adsorption techniques are known to be highly effective for removing high concentrations of antimony from antimony- containing wastewater. Coagulation-precipitation methods have advantages

such as low treatment cost and wide pH applicability (Cao et al., 2017); commonly used coagulants include aluminum salts, iron salts, calcium salts, and polymers (Wu et al., 2011). Ion exchange and membrane separation technologies are highly efficient for Sb(V) removal (Long et al., 2020) and are suitable for industrial wastewater treatment (Nishad et al., 2017). Electro-flocculation (EC) is a convenient and low-sludge-volume technique (Meunier et al., 2004; Holt et al., 2005; Kumarasinghe et al., 2009; Souza et al., 2012; Huang et al., 2020; Prasetyaningrum et al., 2021) with successful applications in treating various wastewaters. Several studies (Song et al., 2014; Cao et al., 2019; Zhou et al., 2022) have successfully applied it. So, to achieve successful removal of antimony, it is important to select the appropriate and economic method depending on the specific wastewater characteristics and treatment requirements.

Micro-electrolysis (ME) is one of the significant electrochemical oxidation-reduction- based wastewater treatment technologies (Xiao et al., 2021). The removal principle of ME is based on the potential difference between the anode and cathode, which forms numerous small galvanic cells that treat the wastewater through oxidation-reduction, flocculation, adsorption, and co-precipitation (Li et al., 2015). This method has the advantages of being economical, environmentally friendly, and easy to operate (Li et al., 2013). Many studies have shown that the performance of ME depends directly on the type of filler used (Jiang et al., 2017; Wang et al., 2018). Wu et al. incorporated manganese into the crystal structure of goethite (FeOOH), resulting in a larger specific surface area of the iron-manganese composite double hydroxide and enhancing its adsorption capacity for metal Cr(VI) (Wu et al., 2007). Similarly, Yang et al. synthesized iron-manganese composite oxides in research on absorbents, and confirmed that their adsorption capacity was higher than that of the iron-based oxidant (FeOOH) or the manganese-based oxidant (MnO_2) (Yang et al., 2019). Furthermore, Zhou et al. introduced an electro-flocculation system employing a composite anode of scrap iron and manganese filings, coupled with an iron plate cathode, for the purpose of Sb(V) removal (Zhou et al., 2022). The results showed that this system formed iron-manganese composite double

hydroxides and had better removal efficiency compared to conventional iron-based electrocoagulation method. Therefore, the construction of an electrochemical oxidation-reduction reaction system using Fe-Mn-C ME for Sb(V) removal has potential for application.

The present study assesses the potential of an innovative ME system comprising waste iron and manganese fillers, in addition to active carbon, for the removal of Sb(V) from aqueous solutions. The investigation pursues two objectives: firstly, to scrutinize the impact of hydraulic retention time (HRT), iron-carbon mass ratio, and manganese proportion on the efficiency of Sb(V) removal; secondly, to perform a microscopic structural analysis of the Fe-Mn-C ME flocs to elucidate the mechanism underlying the removal of Sb(V).

2 Tolerance fluctuation analyses

2.1 Experimental set-up

Fig.1 shows the sketch of the ME experimental setup employed in this study. The system includes the inlet and outlet devices as well as the up-flow reactor. The inlet and outlet device includes an inlet bucket, a peristaltic pump, and an outlet bucket. The up-flow reactor is a cylindrical organic glass vessel of 3.9 L capacity, 10 cm diameter, and 45 cm effective height. The packing layer of the Fe-Mn-C ME reactor is filled with evenly mixed activated carbon particles (4~8 mm), waste iron chips (4~8 mm), and waste manganese chips (4~8mm). Additionally, a small quantity of ceramic particles (1~3 mm) is included to strengthen the mechanical stability. The intercept layer is filled with ceramic particles (5~8 mm) to retain flocculants. A control Fe-C ME reactor without waste manganese chips was also set up based on this configuration. Table S1 presents the concentration of pollutants in the artificially simulated wastewater during continuous flow experiments in two reactors.

2.2 Experimental procedure

To remove the oxide layer from the filler material, a preliminary manual sanding of iron and manganese shavings was performed using sandpaper, followed by a 10-minute immersion in a 3% hydrochloric acid solution. Concurrently, to mitigate the

influence of filler adsorption on the reaction, the activated carbon and ceramic particles were immersed in antimony-containing wastewater for 72 hours to achieve saturation adsorption. Subsequently, the activated carbon and ceramic particles were rinsed with pure water. The pH was adjusted to 6.5 by adding synthetic wastewater and NaOH and HCl solutions. Table S2 displays the designed working conditions, in which our analysis of the influencing factors and mechanisms of Sb(V) removal by Fe-Mn-C ME involved varying the HRT and altering the ratio of iron, carbon, and manganese. In the proposed experimental setup, Stage I is focused on investigating the impact of hydraulic retention time (HRT), while Stage II aims to examine the effects of varying Fe/C/Mn ratios.
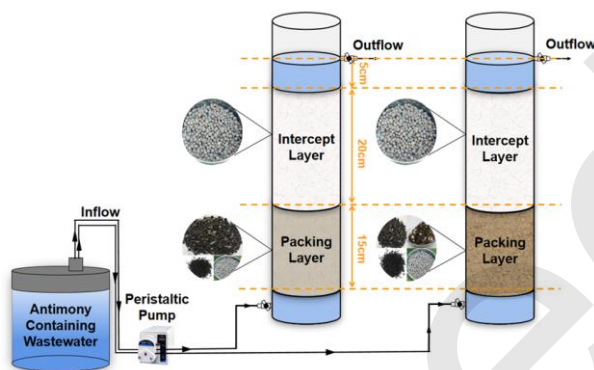

Fig. 1   Schematic diagram of the ME reaction device

2.3   Analytical methods

Samples were collected at scheduled time intervals and analyzed immediately. To ensure statistical reliability, three samples were collected for each sampling event and filtered through 0.22 μm disposable filters. The concentration of Sb(V) in the effluent was measured using an atomic fluorescence photometer (AFS-9320) under the following instrumental conditions: lamp current 75 mA, negative high voltage 300 V, atomizer height 8 mm, furnace temperature 200 ℃, carrier gas Ar (99.99%) at a flow rate of 400 ml/min, and shielding gas Ar (99.99%) at a flow rate of 600 ml/min. The reductants used were 3% (w/v) KBH4 and 0.5% (w/v) NaOH solutions, with carrier solutions of 5% HCl.

The concentrations of Fe(II), Fe(III), and Mn(II) were determined using an atomic absorption spectrometer (ICE3500). The instrumental condi-

tions for Fe(II) and Fe(III) measurements were as follows: maximum lamp current of 15 mA, burner height of 5 mm, slit width of 0.2 nm, air pressure of 1.4 kg/cm2, air flow rate of 5 L/min, and acetylene flow rate of 1.1 L/min. For Mn(II) measurements, the instrumental conditions included a maximum lamp current of 12 mA and a burner height of 8 mm, with all other conditions identical to those used for Fe(II) measurements.

Furthermore, comprehensive characterization was conducted on the generated Fe flocs and Fe-Mn flocs. Phase analysis of Fe flocs and Fe-Mn flocs was performed using powder X-ray diffraction (RIGAKU D/MAX 2550/PC) with Cu Kα radiation (λ = 1.5418 Å), an accelerating voltage of 40 kV, and an applied current of 180 mA. The scanning range was set from 10 to 80º 2θ with a scanning speed of 10 %min and a step size of 0.02 º. The elemental composition of the Fe flocs and Fe-Mn flocs was determined using energy-dispersive X-ray spectroscopy (EDS) with a voltage of 20 kV (FEI FEG650). The Brunauer–Emmett–Teller (BET) specific surface area of the flocs was analyzed using nitrogen adsorption and desorption measurements at 77 K with a nitrogen adsorption apparatus (ASAP 2020 HD88). Finally, X-ray powder diffraction (XPS) was used to determine the composition and chemical states of the flocs (ESCALAB 250Xi) (Yamashita and Hayes, 2008; Yang et al., 2019).

3   Results and discussion

3.1   Sb removal effect under different HRT

Fig.2 shows the variation in removal rates of Sb(Ⅴ) for the Fe-Mn-C ME system and the Fe-C ME system with different HRT.
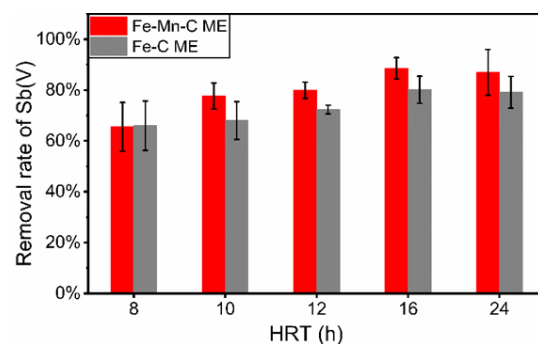

Fig. 2   Variation of Sb(V) removal by Fe-Mn-C and Fe-C ME under different HRT

The removal rates of antimony-containing wastewater by Fe-Mn-C ME and Fe-C ME initially showed an increasing trend. Specifically, when HRT increased from 8h to 16h, the Sb(Ⅴ) removal rate by Fe-Mn-C ME rose from 65.51% to 88.53%, while that of Fe-C ME increased from 66.00% to 80.13%. This can be attributed to the longer contact time between the water flow and the filler. Subsequently, no significant increase in Sb(V) removal was observed even with an extended hydraulic retention time of 24 hours. This is consistent with previous experimental results (Zhang et al., 2016; Wang et al., 2018). Thus, the selection of a suitable HRT is crucial to the effectiveness of the ME system for antimony removal. In addition, when HRT was 8 hours, Fe-Mn-C ME and Fe-C ME systems had similar removal rates. This phenomenon could potentially be attributed to the relatively short HRT, resulting in insufficient contact time between the water flow and the fillers (Sun et al., 2019). As a consequence, both the Fe-Mn-C ME system and the Fe-C ME system may encounter challenges in fully harnessing the oxidative and reductive capabilities of the fillers. However, with an extended HRT of 10-24 hours, the superiority of iron-manganese mixed packing within the micro-electrolysis system became evident. The efficiency of antimony (V) removal through Fe-Mn-C micro-electrolysis (ME) exhibited an increment of 7.60%-9.67% compared to that achieved by Fe-C ME.

3.2   Sb removal effect under different Fe/C mass ratios

Fig.3 depicts the variation in the removal rate of Sb(V) by the Fe-Mn-C ME system under Fe-2C, Fe-C, 2Fe-C, and 3Fe-C working conditions. The results demonstrate that the Fe-Mn-C ME system can maintain a removal efficiency of over 80% for all Fe/C mass ratios tested. The average removal rate of Sb(V) decreases with increasing Fe/C mass ratio, which is consistent with the findings of previous research (Zhang, 2015). This can be attributed to the optimal Fe/C mass ratio where the total area of iron and carbon particles are similar, which favors the formation of macroscopic primary cells and electrode reactions that promote the reaction of ME. (Zhang, 2015; Chen et al., 2018). With higher Fe/C mass ratio ratios, insufficient carbon content in the

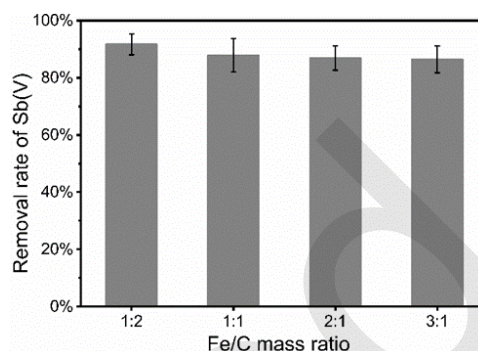packing material diminishes native cell populations, hindering optimal ME outcomes (Zhang, 2015).

Fig. 3   Variation of Sb(V) removal by Fe-Mn-C ME at different Fe/C mass ratios

3.3 Sb removal effect under different manganese additions

Fig.4 illustrates the influence of different amounts of manganese on the removal rate of Sb(V) by the Fe-Mn-C ME system. The removal efficiency of Sb(V) showed an increasing and then decreasing trend with the rise in added manganese. Remarkably, our results demonstrate that at manganese loadings of 10.00%, 11.11%, and 14.29%, the removal efficiency of Sb(V) remained consistently above 80%. However, increasing the manganese loading to 25.00% resulted in a significant decline in the removal efficiency of Sb(V). This decline is probably due to alterations in floc characteristics resulting from excessive manganese content, as will be further analyzed in section 3.4. In light of the above, optimizing manganese addition levels is critical for efficient operation of the Fe-Mn-C ME system. Both excessive and insufficient manganese addition can impair removal performance.
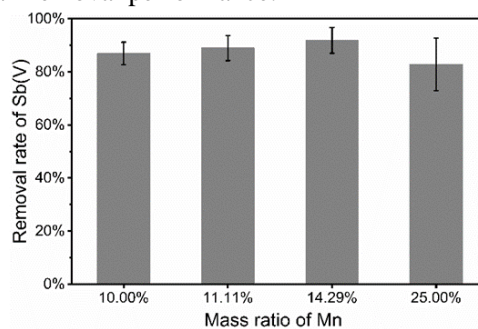

Fig. 4   Variation of Sb(V) removal by Fe-Mn-C ME at different Mn mass ratios

3.4   Characterization of Fe–Mn flocs and Fe flocs

Crystalline structure analysis was carried out using XRD to compare the Fe-Mn flocs or Fe flocs produced by the ME systems under working conditions 0%-Mn, 14.29%-Mn, and 25.00%-Mn. The results are presented in Fig.5.

The Fe flocs formed under the 0%-Mn experimental condition exhibited diffraction peaks around multiple 2θ angles, including 14.2°, 27.1°, 30°, 36.5°, 47.1°, 60.8°, 65.4° and 68.6°, corresponding to the FeOOH crystal planes. Additionally, a distinct diffraction peak was observed at 2θ = 26.3°, indicating the presence of $Fe(OH)_3$ crystal planes, with precise alignment to the diffraction peak angles. Similarly, Fe-Mn flocs produced under conditions of 14.29%-Mn and 25.00%-Mn exhibit the characteristic diffraction peaks of FeOOH and $Fe(OH)_3$. The primary structures of both Fe-Mn flocs and Fe flocs are in the conformation of FeOOH.
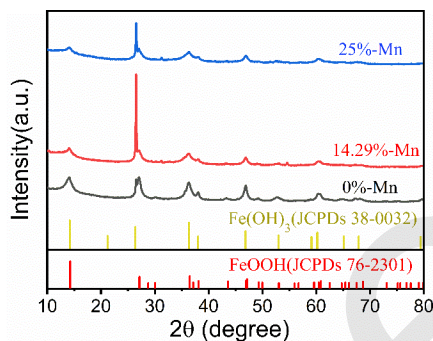

Fig.5   X-ray diffraction (XRD) patterns of Fe-C and Fe-Mn-C flocs

However, we note that the angles of the diffraction peaks of FeOOH in the Fe-Mn flocs produced at 14.29%-Mn and 25.00%-Mn are smaller than those of the standard card values. We also calculated the average grain size of the samples using Scherrer's formula (Muniz et al. 2016), finding that the average grain size of floc obtained for the working condition of 0%-Mn was about 5.7mm, whereas that for the working conditions of 14.29%-Mn and 25.00%-Mn it was approximately 5.2 nm and 4.8 nm, respectively. This suggests that the addition of manganese to the ME system can decrease the average grain size of flocs, which is consistent with previous study (Liu et al., 2018). Sun et al. demonstrated that manganese ions released from the anode were incorporated into the FeOOH crystal structure (Sun et al., 1999). Therefore, manganese incorporation caused the FeOOH crystal structure to shift to-

wards MnOOH, which has the same lattice structure. Then, through lattice substitution and doping with manganese ions, the FeOOH underwent lattice distortion, resulting in a reduction in the grain size and changes in crystallinity (Stiers and Schwertmann 1985). Moreover, the crystal size of Fe-Mn flocs acquired under operational parameters of 14.29%-Mn and 25%-Mn exhibits variation, attributed to the reduction in grain size with the escalating manganese content within the Fe-Mn flocs (Liu et al., 2018).

To further validate the incorporation of manganese ions into the crystal structure of FeOOH, EDS analysis was conducted on both types of flocs to investigate the elemental composition and distribution within the flocs. The results are presented in Fig.S1.

The elemental composition of the Fe-C flocs produced by Fe-C ME at 0%-Mn was mainly composed of O and Fe. On the other hand, the elemental composition of the Fe-Mn-C flocs produced by Fe-Mn-C ME at 14.29%-Mn and 25.00%-Mn included O, Fe, and Mn. The absence of characteristic diffraction peaks of Mn and its compounds in the XRD of the Fe-Mn flocs suggests that lattice substitution of Mn occurred on the surface of δ-FeOOH and Mn was incorporated into the crystal structure of the Fe-Mn flocs. These findings support the hypothesis that the addition of manganese ions alters the composition of the flocs' phases during Fe-Mn-C ME, resulting in the substitution of some iron ions on the surface of the iron flocs with manganese ions (Yang et al., 2019; Wu et al., 2007; Scheinost et al., 2001).

Based on the physical phase analysis and energy spectrum analysis results, it can be inferred that the Fe-Mn-C ME experiments resulted in the formation of Fe-Mn composite double hydroxide flocs.

According to Table S3, the BET specific surface area of Fe-Mn flocs produced under working conditions 14.29%-Mn and 25%-Mn is significantly larger than that of Fe flocs produced under working condition 0%-Mn. This phenomenon is due to the lattice substitution of manganese, which breaks down FeOOH crystals and generates microcrystals, leading to an increase in the specific surface area of Fe-Mn flocs (Gomes et al., 2007). This, in return, results in a higher number of active sites for the adsorption of pollutants and an increase in the removal rate of Sb(Ⅴ) (Jiang et al., 2019). Interestingly, the Fe-Mn floc produced at 14.29%-Mn had a larger

specific surface area than that of 25.00%-Mn, indicating that an excessive amount of Mn reduced the specific surface area of the flocs and made them less effective in the adsorption removal of Sb(V), which is consistent with the variation of Sb(Ⅴ) removal efficiency at different manganese mass percentages previously obtained (Fig.4).

Fig.S2 illustrates the Fe 2p XPS spectra of the flocs generated at working conditions 0%-Mn, 14.29%-Mn, and 25.00%-Mn. The peaks at 710.8eV and 724.4 eV corresponded to Fe $2p^{1/2}$ and Fe $2p^{3/2}$ states of Fe^{2+}, while the peaks at 712.4 eV and 726.4 eV corresponded to Fe $2p^{1/2}$ and Fe $2p^{3/2}$ states of Fe^{3+}. Table S4 presents the percentages of Fe(II) and Fe(III) in flocs under the three experimental conditions (0%-Mn, 14.29%-Mn, 25.00%-Mn), confirming that the content of Fe(II) initially increased significantly then slightly decreased, while the content of Fe(III) initially decreased significantly then slightly increased with increase in manganese content in the ME fillers.

In the XPS spectra of Fe-Mn flocs generated under conditions of 14.29%-Mn and 25.00%-Mn, distinctive peaks exclusively attributed to Mn^{2+} emerge at binding energies of 641.9 eV and 653.2 eV in the Mn 2p high-resolution XPS spectrum. This observation unequivocally signifies the presence of Mn^{2+} ions in the Fe-Mn flocs formed under both conditions. In contrast, examination of the Sb 3d high-resolution XPS spectra of flocs generated under conditions of 0%-Mn, 14.29%-Mn, and 25%-Mn reveals characteristic peaks corresponding to Sb(III) and Sb(V) at binding energies of 530.2 eV and 531.6 eV, respectively.

Table S5 summarizes the contents of Sb(Ⅲ) and Sb(Ⅴ) in the flocs produced under the three working conditions (0%-Mn, 14.29%-Mn, and 25.00%-Mn). The Sb(III) to Sb(V) ratios of flocs obtained through the ME reaction reduced as the amount of manganese in the filler increased. This phenomenon indicates that the Fe-Mn-C ME reaction promotes the reduction of Sb(Ⅴ) to Sb(Ⅲ) more effectively than the Fe-C ME reaction does. Meanwhile, the decrease in the Sb(III)/Sb(V) ratio is consistent with the trend of Sb(V) removal rate (Fig.4), indicating the removal efficiency is related to the reduction reaction. Therefore, optimizing the manganese dosage can enhance the efficiency of Sb(V) reduction removal in the Fe-Mn-C ME reaction.

3.5 Discussion

On the one hand, in Fe-C ME, the electrode potential difference between non-active carbon functioning as the cathode and iron serving as the anode can extend from 0.44 to 1.67 V. Conversely, manganese, when employed as an anode, exhibits a lower standard electrode potential (-1.18 V) compared to iron's standard electrode potential as an anode (-0.44 V), resulting in an electrode potential difference between manganese and carbon that reaches 1.18 to 2.41 V. This augmented electrode potential disparity enhances the driving force of the reaction and consequently elevates the efficiency of electron transfer. Consequently, the potential differences between iron and carbon, as well as between manganese and carbon, facilitate efficient electron transfer and enhance the redox activity of the electrolyte solution.

On the other hand, there exists a potential difference between iron and manganese (Huang and Zhang, 2020), which contributes to further improving electron transfer efficiency and redox activity. As a result, the Fe-Mn-C ME system constitutes Fe-C primary cells, Mn-C primary cells, and Fe-Mn primary cells, increasing the number of primary cells and promoting electron transfer and the release of Fe(Ⅱ) and reduced hydrogen (Duan et al., 2022). This is why the removal efficiency of Sb(V) by the Fe-Mn-C ME system is higher than that of the Fe-C ME system (Fig 2). Moreover, as a good conductor, manganese can facilitate electron transfer between iron and carbon (Tan et al., 2016), which further enhances the reduction and removal of antimony.

In conjunction with XPS analysis of the Fe-Mn flocs in Fig.S2 and Table S4, it was found that the Fe(Ⅱ) content in the flocs increases with increasing manganese content in the ME reaction system, while the Fe(Ⅲ) content decreases. This suggests that further redox reactions occur between Mn0 and Fe(Ⅲ).

The Fe(Ⅱ) and reduced hydrogen produced by the ME system exhibit strong reduction activity (Luo et al., 2014; X and Y, 2017), which promotes the reduction of some surface-bound Sb(Ⅴ) to Sb(Ⅲ), as confirmed by XPS analysis of both the Fe-Mn and Fe flocs. Due to low solubility and a propensity for hydrolysis and precipitation in aqueous solutions, Sb(III) can be effectively adsorbed and removed by the flocs (Wu et al., 2020).

Adsorption also plays an important role in the removal of Sb(V). During the experiment, a large amount of flocs was generated on the surface of the filler and at the bottom of the reactor, due to the excellent flocculation characteristics of the Fe(Ⅱ) and Fe(Ⅲ) generated by anodic ionization, which can hydrolyze and form complexes to produce flocs such as $Fe(OH)_3$ and FeOOH. Furthermore, the robust redox capability of the Fe-Mn-C ME system facilitates the transformation of $Fe(OH)_3$ into FeOOH. XRD and EDS analyses confirmed the formation of iron-manganese composite hydroxides, and BET analysis showed that iron-manganese composite hydroxides have a larger specific surface area and higher adsorption activity than pure $Fe(OH)_3$ or FeOOH. EDS images also revealed the presence of antimony ions on the surface of the Fe-Mn flocs, corroborating the adsorption of Sb from wastewater onto the flocs.

In summary, during the Fe-Mn-C ME reaction, some Sb(V) is adsorbed and removed by the iron-manganese composite hydroxide flocs with good adsorption performance, while another portion of Sb(V) is reduced to Sb(III) by Fe(Ⅱ) and generates $Sb(OH)_3$ precipitate during coagulation, which is removed by adsorption and co-precipitation with the flocs. The detailed chemical reaction equations involved can be found in the supplementary materials.

4   Simulation results and discussion

In this study, a composite material made of waste iron scraps, waste manganese scraps and activated carbon was used to remove Sb(V) from synthetic wastewater through micro-electrolysis. The results showed that the iron-manganese-carbon micro-electrolysis method significantly improved efficiency of removal of Sb(V) compared to the conventional iron-carbon micro-electrolysis method. Under the experimental conditions of a hydraulic retention time of 10-24 h, pH of 6.5, iron-carbon mass ratio of 1.6:1, and initial Sb(V) concentration of 1 mg/L, the average removal rate of Sb(V) by iron-manganese-carbon micro-electrolysis was 7.60-9.67% higher than that of iron-carbon micro-electrolysis, reaching a maximum of 91.85%.

The influence of iron to carbon mass ratio and manganese mass ratio on Sb(V) removal were also further investigated. The results showed that the removal rate of Sb(V) decreased with increasing iron to carbon mass ratio. However, the removal efficiency initially increased and then decreased with increasing manganese content, reaching a maximum value of 14.29% at an iron-carbon ratio of 1:2.

XRD and EDS analysis indicated that the composition of the iron-manganese flocs was mainly manganese-substituted FeOOH. BET surface area analysis confirmed that the iron-manganese flocs had a larger surface area compared to iron flocs, which contributed to their improved removal efficiency. XPS analysis showed that the presence of manganese in the micro-electrolysis material increased the Fe(Ⅱ) content and decreased the Fe(Ⅲ) content in the flocs, promoting the forward reduction of Sb(V). Mechanistic analysis suggested that in the iron-manganese-carbon micro-electrolysis system, part of the Sb(V) was removed via adsorption onto the iron-manganese composite hydrous oxide flocs, which had good adsorption properties, while the rest was reduced to Sb(III) and precipitated as $Sb(OH)_3$ during coagulation, which was then removed via adsorption and co-precipitation with the flocs.

Author contributions

All authors contributed to the study conception and design. Shangkun DING: Conceptualization; Investigation; Writing-Original draft preparation. Saihua HUANG: Supervision; Writing-Reviewing and Editing. Yiping ZHANG: Methodology; Supervision. Yongchao ZHOU: Conceptualization; Methodology.

Conflict of interest

Shangkun DING, Saihua HUANG, Yiping ZHANG, and Yongchao ZHOU declare that they have no conflict of interest.

References

Cao D, Zeng H, Yang B, et al., 2017. Mn assisted electrochemical generation of two-dimensional Fe-Mn layered double hydroxides for efficient Sb(V) removal. *Journal of Hazardous Materials*, 336:33-40. https://doi.org/10.1016/j.jhazmat.2017.04.034

Cao D, Guo T, Zhao X, 2019. Treatment of Sb(V) and CO(II)

containing wastewater by electrocoagulation and enhanced Sb(V) removal with CO(II) presence. *SEPARATION AND PURIFICATION TECHNOLOGY*, 227 https://doi.org/10.1016/j.seppur.2019.05.091

Chen F, Li X, Luo Z, et al., 2018. Advanced treatment of copper smelting wastewater by the combination of internal micro-electrolysis and electrocoagulation. *Separation Science and Technology*, 53(16):2639-2646. https://doi.org/10.1080/01496395.2018.1463265

Duan C, Huang X, Gao J, et al., 2022. Iron-carbon (fe-c) micro-electrolysis coupling with anaerobic-anoxic-oxic (a2/o) process: Nitrogen and phosphorus removal performance and microbial characteristics. *Journal of Environmental Chemical Engineering*, 10(2):107235. https://doi.org/10.1016/j.jece.2022.107235

Fei J-C, Min X-B, Wang Z-X, et al., 2017. Health and ecological risk assessment of heavy metals pollution in an antimony mining region: A case study from south china. *Environmental Science and Pollution Research*, 24(35):27573-27586. https://doi.org/10.1007/s11356-017-0310-x

Gannon K, Wilson DJ, 1986. Removal of antimony from aqueous systems. *Separation Science and Technology*, 21(5):475-493. https://doi.org/10.1080/01496398608056130

Gomes JaG, Daida P, Kesmez M, et al., 2007. Arsenic removal by electrocoagulation using combined al–fe electrode system and characterization of products. *Journal of Hazardous Materials*, 139(2):220-231. https://doi.org/10.1016/j.jhazmat.2005.11.108

Guo X, Wu Z, He M, 2009. Removal of antimony(v) and antimony(iii) from drinking water by coagulation–flocculation–sedimentation (CFS). *Water Research*, 43(17):4327-4335. https://doi.org/10.1016/j.watres.2009.06.033

Hasan MB, Al-Tameemi IM, Abbas MN, 2021. Orange peels as a sustainable material for treating water polluted with antimony. *Journal of Ecological Engineering*, 22(2):25-35. https://doi.org/10.12911/22998993/130632

Holt PK, Barton GW, Mitchell CA, 2005. The future for electrocoagulation as a localised water treatment technology. *Chemosphere*, 59(3):355-367. https://doi.org/10.1016/j.chemosphere.2004.10.023

Huang J, Zhang H, 2020. Redox reactions of iron and manganese oxides in complex systems. *Frontiers of Environmental Science & Engineering*, 14(5):76. https://doi.org/10.1007/s11783-020-1255-8

Jiang HR, Shyy W, Wu MC, et al., 2019. A bi-porous graphite felt electrode with enhanced surface area and catalytic activity for vanadium redox flow batteries. *Applied Energy*, 233:105-113. https://doi.org/10.1016/j.apenergy.2018.10.033

Jiang YH, Li M, Yan AP, 2017. Enhanced manganese-carbon microelectrolysis for pretreatment of gasification wastewater from synthetic ammonia industry.

Environmental Engineering Science, 34(4):291-298. https://doi.org/10.1089/ees.2016.0187

Kang M, Kamei T, Magara Y, 2003. Comparing polyaluminum chloride and ferric chloride for antimony removal. *Water Research*, 37(17):4171-4179. https://doi.org/10.1016/S0043-1354(03)00351-8

Kumarasinghe D, Pettigrew L, Nghiem LD, 2009. Removal of heavy metals from mining impacted water by an electrocoagulation-ultrafiltration hybrid process. *Desalination and Water Treatment*, 11(1-3):66-72. https://doi.org/10.5004/dwt.2009.844

Li FB, Lin T, Li Q, et al., 2013. Research on cavitation and impinging stream microelectrolysis reactor for treating organic wastewater. *Advances in Materials and Materials Processing, Pts 1-3*, 652-654:1692-1695. https://doi.org/10.4028/www.scientific.net/AMR.652-654.1692

Li JY, Zheng BH, He YZ, et al., 2018. Antimony contamination, consequences and removal techniques: A review. *Ecotoxicology and Environmental Safety*, 156:125-134. https://doi.org/10.1016/j.ecoenv.2018.03.024

Li T, Li T, Xiong H, et al., 2015. Factors influencing hydroquinone degradation in aqueous solution using a modified microelectrolysis method. *Water Science and Technology*, 71(3):397-404. https://doi.org/10.2166/wst.2014.534

Liu H, Lu XC, Li M, et al., 2018. Structural incorporation of manganese into goethite and its enhancement of pb(ii) adsorption. *Environmental Science & Technology*, 52(8):4719-4727. https://doi.org/10.1021/acs.est.7b05612

Long X, Wang X, Guo X, et al., 2020. A review of removal technology for antimony in aqueous solution. *Journal of Environmental Sciences*, 90:189-204. https://doi.org/10.1016/j.jes.2019.12.008

Luo J, Song G, Liu J, et al., 2014. Mechanism of enhanced nitrate reduction via micro-electrolysis at the powdered zero-valent iron/activated carbon interface. *Journal of Colloid and Interface Science*, 435:21-25. https://doi.org/10.1016/j.jcis.2014.08.043

Meunier N, Drogui P, Gourvenec C, et al., 2004. Removal of metals in leachate from sewage sludge using electrochemical technology. *ENVIRONMENTAL TECHNOLOGY*, 25(2):235-245. https://doi.org/10.1080/09593330409355457

Mitsunobu S, Takahashi Y, Terada Y, et al., 2010. Antimony(v) incorporation into synthetic ferrihydrite, goethite, and natural iron oxyhydroxides. *Environmental Science & Technology*, 44(10):3712-3718. https://doi.org/10.1021/es903901e

Muniz FTL, Miranda MaR, Dos Santos CM, et al., 2016. The scherrer equation and the dynamical theory of x-ray diffraction. *Acta Crystallographica a-Foundation and Advances*, 72:385-390. https://doi.org/10.1107/S205327331600365x

Nishad PA, Bhaskarapillai A, Velmurugan S, 2017. Towards finding an efficient sorbent for antimony: Comparative investigations on antimony removal properties of potential antimony sorbents. *International Journal of Environmental Science and Technology*, 14(4):777-784. https://doi.org/10.1007/s13762-016-1181-2

Ozdemir N, Soylak M, Elcib L, et al., 2004. Speciation analysis of inorganic sb(iii) and Sb(V) ions by using mini column filled with amberlite xad-8 resin. *Analytica Chimica Acta*, 505(1):37-41. https://doi.org/10.1016/S0003-2670(03)00353-2

Prasetyaningrum A, Ariyanti D, Widayat W, et al., 2021. Copper and lead ions removal by electrocoagulation: Process performance and implications for energy consumption. *INTERNATIONAL JOURNAL OF RENEWABLE ENERGY DEVELOPMENT-IJRED*, 10(3):415-424. https://doi.org/10.14710/ijred.2021.31665

Riveros PA, Dutrizac JE, Lastra R, 2008. A study of the ion exchange removal of antimony(iii) and antimony(v) from copper electrolytes. *Canadian Metallurgical Quarterly*, 47(3):307-315. https://doi.org/DOI 10.1179/cmq.2008.47.3.307

Saito T, Tsuneda S, Hirata A, et al., 2004. Removal of antimony(iii) using polyol-ligand-containing porous hollow-fiber membranes. *Separation Science and Technology*, 39(13):3011-3022. https://doi.org/10.1081/SS-200033727

Scheinost AC, Stanjek H, Schulze DG, et al., 2001. Structural environment and oxidation state of mn in goethite-groutite solid-solutions. *American Mineralogist*, 86(1-2):139-146.

Song P, Yang Z, Xu H, et al., 2014. Investigation of influencing factors and mechanism of antimony and arsenic removal by electrocoagulation using fe-al electrodes. *INDUSTRIAL & ENGINEERING CHEMISTRY RESEARCH*, 53(33):12911-12919. https://doi.org/10.1021/ie501727a

Song P, Yang Z, Zeng G, et al., 2015. Optimization, kinetics, isotherms, and thermodynamics studies of antimony removal in electrocoagulation process. *Water Air and Soil Pollution*, 226(11):380. https://doi.org/10.1007/s11270-015-2615-z

Souza KR, Silva DR, Mata W, et al., 2012. Electrochemical technology for removing heavy metals present in synthetic produced water. *LATIN AMERICAN APPLIED RESEARCH*, 42(2):141-147.

Stiers W, Schwertmann U, 1985. Evidence for manganese substitution in synthetic goethite. *Geochimica et Cosmochimica Acta*, 49(9):1909-1911. https://doi.org/Doi 10.1016/0016-7037(85)90085-7

Sun XH, Doner HE, Zavarin M, 1999. Spectroscopy study of arsenite [as(iii)] oxidation on mn-substituted goethite. *Clays and Clay Minerals*, 47(4):474-480.

Sun ZH, Xu ZH, Zhou YW, et al., 2019. Effects of different scrap iron as anode in fe-c micro-electrolysis system for textile wastewater degradation. *Environmental Science and Pollution Research*, 26(26):26869-26882. https://doi.org/10.1007/s11356-019-05931-3

Tan FK, Hassan J, Wahab ZA, et al., 2016. Electrical conductivity and dielectric behaviour of manganese and vanadium mixed oxide prepared by conventional solid state method. *Engineering Science & Technology An International Journal*, :2081-2087.

Ungureanu G, Santos S, Boaventura R, et al., 2015. Arsenic and antimony in water and wastewater: Overview of removal techniques with special reference to latest advances in adsorption. *Journal of Environmental Management*, 151:326-342. https://doi.org/10.1016/j.jenvman.2014.12.051

Wang Y, Feng M, Liu Y, 2018. Preparation and application of aluminum-carbon microelectrolysis materials. *Journal of Environmental Engineering*, 144(4):04018016. https://doi.org/10.1061/(ASCE)EE.1943-7870.0001351

Wu F, Fu Z, Liu B, et al., 2011. Health risk associated with dietary co-exposure to high levels of antimony and arsenic in the world's largest antimony mine area. *Science of The Total Environment*, 409(18):3344-3351. https://doi.org/10.1016/j.scitotenv.2011.05.033

Wu WC, Wang SL, Tzou YM, et al., 2007. The adsorption and catalytic transformations of chromium on mn substituted goethite. *Applied Catalysis B-Environmental*, 75(3-4):272-280. https://doi.org/10.1016/j.apcatb.2007.04.026

Wu X, Lv C, Yu S, et al., 2020. Uranium (vi) removal from aqueous solution using iron-carbon micro-electrolysis packing. *SEPARATION AND PURIFICATION TECHNOLOGY*, 234:116104. https://doi.org/10.1016/j.seppur.2019.116104

X Z, Y W, 2017. Application of coupled zero-valent iron/biochar system for degradation of chlorobenzene-contaminated groundwater. *Water science and technology : a journal of the International Association on Water Pollution Research*, 75(3-4) https://doi.org/10.2166/wst.2016.503

Xiao Y, Shao Y, Luo M, et al., 2021. Optimized study and column experiments on treatment process of metronidazole pharmaceutical wastewater by microelectrolysis and fenton oxidation. *Water, Air, & Soil Pollution*, 232(5):182. https://doi.org/10.1007/s11270-021-05117-z

Yamashita T, Hayes P, 2008. Analysis of xps spectra of fe^{2+} and fe^{3+} ions in oxide materials. *Applied Surface Science*, 254(8):2441-2449. https://doi.org/10.1016/j.apsusc.2007.09.063

Yang KL, Liu YL, Li YZ, et al., 2019. Applications and characteristics of fe-mn binary oxides for Sb(V) removal in textile wastewater: Selective adsorption and the fixed-bed column study. *Chemosphere*, 232:254-263. https://doi.org/10.1016/j.chemosphere.2019.05.194

Zhang Q, 2015. Treatment of oilfield produced water using fe/c micro-electrolysis assisted by zero-valent copper

and zero-valent aluminium. *ENVIRONMENTAL TECHNOLOGY*, 36(4):515-520. https://doi.org/10.1080/09593330.2014.952678

Zhang X, Yue Q, Yue D, et al., 2015. Application of fe⁰/c/clay ceramics for decoloration of synthetic acid red 73 and reactive blue 4 wastewater by micro-electrolysis. *Frontiers of Environmental Science & Engineering*, 9(3):402-410. https://doi.org/10.1007/s11783-014-0659-8

Zhou Y, Zheng W, Zhang W, et al., 2022. Effective removal of Sb(V) from aqueous solutions by electrocoagulation with composite scrap iron-manganese as an anode. *Environmental Science and Pollution Research*, 29(38):58088-58096. https://doi.org/10.1007/s11356-022-20033-3

Zhu J, Wu F, Pan X, et al., 2011. Removal of antimony from antimony mine flotation wastewater by electrocoagulation with aluminum electrodes. *Journal of Environmental Sciences*, 23(7):1066-1071. https://doi.org/10.1016/S1001-0742(10)60550-5

Electronic supplementary materials

Table S1
Table S2
Table S3
Table S4
Table S5
Fig. S1
Fig. S2

中文概要

题　　目：以废铁锰为填料的微电解技术高效除锑研究

作　　者：丁尚坤[1]、黄赛花[2]、张仪萍[1]、周永潮[1]

机　　构：[1]浙江大学,市政工程研究所,中国杭州,310058；
[2]浙江水利水电学院，中国杭州，310018

目　　的：近年来锑污染日益严重，因此亟需探索出经济有效的方法除锑。本研究提出了一种经济环保、操作简单、效果稳定的微电解除锑技术，旨在探究其去除效果、影响因素及去除机理。

创新点：1. 提出了基于铁锰碳填料的微电解系统除锑；2. 探究了铁锰碳微电解体系除锑的主要机理，包括氧化还原作用、吸附和共沉淀作用。

方　　法：1. 探究不同水力停留时间 HRT，铁碳质量比、锰含量下，铁锰碳微电解去除性能的变化；2. 对微电解产生的絮体进行 XRD、EDS、BET、XPS 等微观结构分析，探究铁锰复合双氢氧化物的形成和 Sb(V)去除的机理。

结　　论：1. 当水力停留时间为 10-24h，填料投加量为 250g/L，pH 值为 6.5，铁碳比为 1.6:1，Sb(V)初始浓度 1mg/L 时，铁锰碳微电解的 Sb(V) 平均去除率比铁碳微电解高出 7.60%-9.67%。2. 最佳实验工况下，铁锰碳微电解法的 Sb(V)去除率可达 91.85%。3. 机理分析表明，在铁锰碳微电解反应中，部分 Sb(V)被反应生成的具有良好吸附性能的铁锰复合双氢氧化物絮体吸附去除，另一部分被还原为 Sb(III)，在混凝过程中生成 Sb(OH)₃ 沉淀，通过絮体的吸附与共沉淀反应去除。

关键词：锑、铁、锰、微电解、机理